



UNIVERSITY OF LEEDS

This is a repository copy of *Constraints on the functional form of the critical deposition velocity in solid-liquid pipe flow at low solid volume fractions*.

White Rose Research Online URL for this paper:  
<http://eprints.whiterose.ac.uk/83455/>

Version: Accepted Version

---

**Article:**

Rice, HP, Fairweather, M, Peakall, J et al. (3 more authors) (2015) Constraints on the functional form of the critical deposition velocity in solid-liquid pipe flow at low solid volume fractions. *Chemical Engineering Science*, 126. 759 - 770. ISSN 0009-2509

<https://doi.org/10.1016/j.ces.2014.12.039>

---

**Reuse**

Unless indicated otherwise, fulltext items are protected by copyright with all rights reserved. The copyright exception in section 29 of the Copyright, Designs and Patents Act 1988 allows the making of a single copy solely for the purpose of non-commercial research or private study within the limits of fair dealing. The publisher or other rights-holder may allow further reproduction and re-use of this version - refer to the White Rose Research Online record for this item. Where records identify the publisher as the copyright holder, users can verify any specific terms of use on the publisher's website.

**Takedown**

If you consider content in White Rose Research Online to be in breach of UK law, please notify us by emailing [eprints@whiterose.ac.uk](mailto:eprints@whiterose.ac.uk) including the URL of the record and the reason for the withdrawal request.



[eprints@whiterose.ac.uk](mailto:eprints@whiterose.ac.uk)  
<https://eprints.whiterose.ac.uk/>

Hugh P. Rice\*<sup>1</sup>, Michael Fairweather<sup>1</sup>, Jeffrey Peakall<sup>2</sup>, Timothy N. Hunter<sup>1</sup>, Bashar Mahmoud<sup>1</sup> and Simon R. Biggs<sup>a1</sup>

<sup>1</sup> School of Process, Environmental and Materials Engineering

<sup>2</sup> School of Earth and Environment

University of Leeds, Leeds LS2 9JT, United Kingdom

\* Correspondence to h.p.rice@leeds.ac.uk

## **Constraints on the functional form of the critical deposition velocity in solid-liquid pipe flow at low solid volume fractions**

### **Abstract**

Of the various transition velocities that delineate flow regimes in multiphase pneumatic and hydraulic conveying, the critical deposition velocity is important because it separates depositing and non-depositing flows. However, no distinction has been made between the dependence of the critical deposition velocity on physical parameters and flow conditions at low solid volume fractions and in the limit of zero volume fraction, which are distinct mathematically. Here, the two cases are analysed separately, and a general functional form in terms of the particle Reynolds number and Archimedes number is proposed that is valid up to volume fractions of several per cent. An ultrasonic method for determining the critical value of the particle Reynolds number is presented, and results for four particle types at several nominal volume fractions (0.5, 1 and 3 % by volume) are combined with a number of data from the literature. The resulting expressions are found to compare well with several similar correlations for the critical deposition velocity and other transition velocities, and, unlike a recent best-fit approach for the pick-up velocity, incorporate an explicit dependence on volume fraction, to which the critical deposition velocity is most sensitive at very low volume fractions. Lastly, it is found that the functional forms for the critical deposition velocity in the literature are unable to reproduce the available data at higher volume fractions, and a number of suggestions are made for resolving this issue.

---

<sup>a</sup> Current address: Faculty of Engineering, Architecture and Information Technology, University of Queensland, Brisbane, QLD 4072, Australia

## 1. Introduction

Flow of solid-liquid suspensions can be categorised as (Crowe, 2006; Doron and Barnea, 1995; Wasp *et al.*, 1977): non-settling, in which the solid particles remain suspended in the carrier fluid; unhindered-settling, in which suspended particles can freely settle under the influence of gravity (corresponding broadly to low-concentration flows); and hindered-settling, in which hindrance to downward-moving particles is provided by upward-moving carrier fluid in order to conserve mass. Alternatively, five flow regimes, and various combinations thereof, can be identified as (Crowe, 2006; Peker and Helvacı, 2007):

1. Homogeneous (or pseudo-homogeneous), in which all particles are suspended and the concentration is constant across the diameter of the conduit;
2. Heterogeneous, in which a concentration gradient exists in the suspension;
3. Flow with a moving bed, or sometimes saltation flow or “two-layer” flow, in which some fraction of the suspended particles has settled and formed a sediment bed that moves along the channel;
4. Flow with a stationary bed, or sometimes “three-layer” flow, in which at least part of the sediment is stationary relative to the channel; or
5. Plug flow, in which the solids span the diameter of the channel and move *en masse*.

Idealised versions of these flow regimes are illustrated in Table 1.

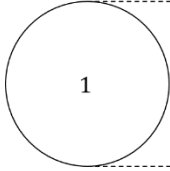
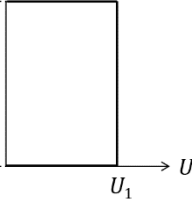
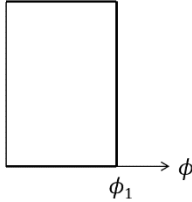
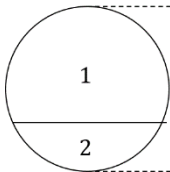
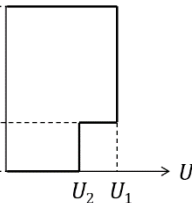
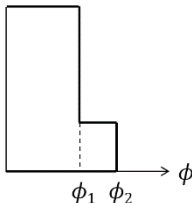
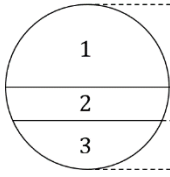
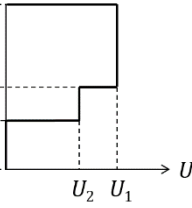
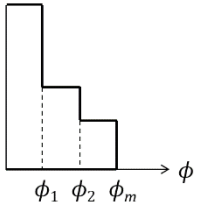
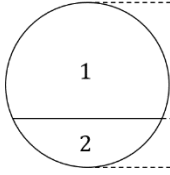
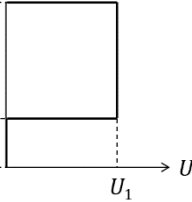
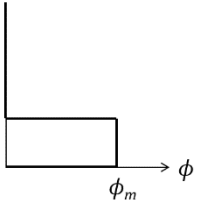
Table 1: Description of idealised flow regimes. Adapted from Gillies and Shook (1991) and Doron and Barnea (1996). $U$ is axial flow velocity; $\phi$ is volume fraction of solids.				
Case	Description	Cross-section	Velocity, $U$	Volume fraction, $\phi$
1	Homo- or heterogeneous or plug flow, fully suspended			
2	Moving bed/shear layer			

Table 1: Description of idealised flow regimes. Adapted from Gillies and Shook (1991) and Doron and Barnea (1996). $U$ is axial flow velocity; $\phi$ is volume fraction of solids.				
Case	Description	Cross-section	Velocity, $U$	Volume fraction, $\phi$
3	Stationary bed with moving bed/shear layer			
4	No particle motion and/or no flow			

The flow regimes described above are commonly delineated by a number of transition velocities, and the focus of the present study is specifically on the transition velocity between depositing and non-depositing flows. However, such transition velocities have a wide variety of definitions (Crowe, 2006; Harbottle *et al.*, 2011; Peker and Helvacı, 2007; Rabinovich and Kalman, 2011), and some ambiguity exists. For example, Spells (1955) defined a “standard velocity” at which the pressure gradient for a slurry and its “equivalent true fluid” – *i.e.* pseudo-fluid – are equal. Indeed, the pressure gradient – specifically the velocity at which the pressure gradient reaches a minimum – is invoked in a number of definitions of the transition velocity between depositing and non-depositing suspensions. Although this minimum-pressure point has been equated with the critical deposition velocity in some studies (Poloski *et al.*, 2010), in others a distinction has been made: Bain and Bonnington (1970) found that the minimum-pressure velocity generally exceeded the critical deposition velocity.

In a recent and comprehensive review of a very broad range of literature (Soeptyan *et al.*, 2014), 44 models of various transition velocities and shear stress at low solids volume fractions ( $0 < \phi < 10^{-4}$ ) were described. Various definitions of the deposition velocity were given, as follows, based on a number of other studies (Gruesbeck *et al.*, 1979; Hayden *et al.*, 2003; Oroskar and Turian, 1980; Rabinovich and Kalman, 2009, 2011; Zenz, 1964): the critical velocity, which delineates the onset of settling and full suspension; the pick-up velocity, at which particles initially having been at rest on the surface of a particle bed “begin their motion within the fluid”; the incipient motion velocity, at which a single particle is picked up; the saltation velocity, which is the minimum flow velocity at which no particles settle on the bottom of the pipe; and the equilibrium velocity, at which the

rate of settling onto the bottom of the pipe balances the rate of pick-up from it. In fact, in one review article, the incipient motion velocity has been categorised as a type of pick-up velocity, and the minimum-pressure velocity as a type of saltation velocity (Rabinovich and Kalman, 2011).

In the present study, a method is presented for determining the mean flow velocity corresponding to zero settled bed depth by extrapolation of experimental data recorded over a range of bed depths. This particular transition velocity, referred to hereafter as the critical deposition velocity,  $U_c$ , corresponds most closely to the critical velocity or saltation velocity of Soepyan *et al.* (2014) and the limit deposit velocity of Peker and Helvacı (2007). It is the determination of the dependence of the critical deposition velocity on particle and flow properties that is the main objective of this study.

## 2. Functional form of critical deposition velocity: review

A standardised form for the critical deposition velocity, based on that for the pick-up velocity given by Soepyan *et al.* (2014), can be expressed as follows:

$$\text{Re}_{pc} = f(\text{Ar})g(\phi, \phi_c, d, D, \rho_s, \rho_f, \nu, C_D), \quad [1]$$

where  $\text{Re}_{pc}$  is the particle Reynolds number corresponding to the critical deposition velocity,  $U_c$ , such that:

$$\text{Re}_{pc} = \frac{U_c d}{\nu}, \quad [2]$$

$f$  is a function incorporating the dependence on the Archimedes number,  $\text{Ar}$ , defined below;  $g$  is that for the remaining flow and particle properties;  $\phi$  is the solids volume fraction;  $\phi_c$  is a critical value of  $\phi$ , such as that in the moving bed,  $\phi_{mb}$ , or the maximum packing fraction,  $\phi_m$ ;  $d$  is the particle diameter;  $D$  is the pipe diameter;  $\rho_s$  and  $\rho_f$  are the densities of the solid and fluid phases, respectively;  $\nu$  is the kinematic viscosity of the fluid; and  $C_D$  is the drag coefficient of the particles. The maximum packing fraction – *i.e.* the maximum possible volume fraction that can be occupied by settled particles in a bed – was not referred to in any of the models described by Soepyan *et al.* (2014), but is posited here as a parameter that is very likely to influence the form of  $g$ , as described later. Lastly, the Archimedes number is defined as follows:

$$\text{Ar} = \frac{g_n d^3 (S - 1)}{\nu^2} \quad [3]$$

where  $g_n$  is the acceleration due to gravity (not to be confused with  $g$  in Equation [1] and elsewhere) and  $S$  is the specific gravity of the particles, such that:

$$S = \frac{\rho_s}{\rho_f}. \quad [4]$$

$\text{Re}_p$  can therefore be regarded as the ratio of inertial to viscous forces on a particle, and  $\text{Ar}$  the ratio of gravitational to buoyancy forces. The particle Reynolds number,  $\text{Re}_p$ , and the Archimedes number,  $\text{Ar}$ , were chosen by Soepyan *et al.* (2014) “because they include some of the most significant forces for particle transport”.

The functional form given in Equation [1] differs from that suggested by Rabinovich and Kalman (2011), which is as follows:

$$\text{Re}_{pt}^* = a(\text{Ar}^*)^b \quad [5]$$

where  $\text{Re}_{pt}^*$  and  $\text{Ar}^*$  are modified versions of  $\text{Re}_{pt}$  and  $\text{Ar}$  that take into account volume fraction, pipe diameter and particle sphericity/shape, with the subscript “ $t$ ” in  $\text{Re}_{pt}$  representing a general transition value of  $\text{Re}_p$ , of which  $\text{Re}_{pc}$  (critical deposition value) and  $\text{Re}_{pp}$  (pick-up) are examples;  $a$  and  $b$  are arbitrary coefficients.

At this point, it is necessary to identify an important distinction that has not generally been upheld in the literature, namely that between the functional form of  $g$  at low values of the volume fraction,  $\phi$ , and in the limit of zero volume fraction, *i.e.* as  $\phi \rightarrow 0$ . That these two regimes are strictly mathematically distinct has a number of important implications for the subject of critical velocity correlations of the kind expressed in Equation [1], as will be explained in the remainder of this study. Hereafter, the subscript “0” is used to indicate the value of a function or parameter in the limit  $\phi \rightarrow 0$ . For example, the particle Reynolds number at deposition in the limit of zero volume fraction is as follows:

$$\text{Re}_{pc0} = \lim_{\phi \rightarrow 0} \text{Re}_{pc}. \quad [6]$$

It is necessary to specify the limit  $\phi \rightarrow 0$ , rather than the simpler condition  $\phi = 0$ , in this context because the volume fraction,  $\phi$ , is only defined on the interval  $0 < \phi < 1$  in liquid-

solid suspensions: at  $\phi = 0$ , a pure fluid is obtained, while at  $\phi = 1$ , a pure powder/solid. The critical velocity,  $U_c$ , and quantities derived from it, such as  $Re_p$ , are therefore defined on the same interval.

The standardisation procedure performed by Soepyan *et al.* (2014) allowed a large number of models to be compared directly and ranked according to their ability to recreate the experimental data available in the literature (a total of 117 data for horizontal, solid-liquid pipe flow), both before and after “fine-tuning”, that is, optimisation of parameters. The most important observations and conclusions to be drawn from the analysis performed by Soepyan *et al.* (2014) are as follows. Of the three models identified as most successful *before* optimisation (*i.e.* with the values of the model parameters as given in the original models), none contained a dependence on the particle volume fraction,  $\phi$ . The models were those of Mantz (1977), Rabinovich and Kalman (2007) and Dey (1999), *i.e.* models 6, 16 and 42 (and functional forms 3, 10 and 33), respectively, in the nomenclature of Soepyan *et al.* (2014). After optimisation, the ten most highly-ranked models had no or a very weak dependence on the volume fraction,  $\phi$ , and several other parameters. More specifically, five of the ten most successful models reduced to an identical form, namely:

$$Re_{pp0} = 7.90Ar^{0.41}, \quad [7]$$

where it is important to note that  $Re_{pp0}$  is the Reynolds number corresponding to the pick-up velocity, and not the critical deposition velocity,  $Re_{pc}$ . Soepyan *et al.* (2014) only analysed the pick-up velocity, and not the critical deposition velocity, in hydraulic flows, but the functional form they proposed is adopted in this study, by analogy (Rabinovich and Kalman, 2011).

Soepyan *et al.* (2014) used only data in the range  $0 < \phi < 10^{-4}$  for their optimisation procedure, so it is not surprising that the most successful functional forms contained little or no dependence on  $\phi$ . If the “ $\Delta$ ” operator is used to indicate an increment, then the relative variation in  $Re_{pc}$  over a small range can be expressed as  $\Delta Re_{pc}/Re_{pc}$ . If the derivative with respect to volume fraction,  $\phi$ , is denoted by an apostrophe, and the following approximation is made:

$$Re'_{pc} = \frac{\partial Re_{pc}}{\partial \phi} \approx \frac{\Delta Re_{pc}}{\Delta \phi}, \quad [8]$$

then the variation in  $Re_{pc}$  is as follows:

$$\frac{\Delta Re_{pc}}{Re_{pc}} \approx \Delta\phi \frac{Re'_{pc}}{Re_{pc}}. \quad [9]$$

Taking  $Re'_{pc}/Re_{pc}|_{\phi \ll 1} = O(10)$ , as determined later (see Table 3 and the associated text) and  $\Delta\phi = 10^{-4}$  (*i.e.* over the range  $0 < \phi < 10^{-4}$ ), then  $\Delta Re_{pc}/Re_{pc} = O(10^{-3})$ , *i.e.* 0.1 %, which is negligible. This argument applies equally to correlations expressed in terms of  $U_c$ ,  $Fr$  or other similar measured flow parameters. It would, then, be extremely difficult to determine the dependence of the critical velocity on  $\phi$  from such low- $\phi$  data alone. It is with the preceding arguments in mind that the results of the optimisation performed by Soepyan *et al.* (2014) – specifically the functional form to which five of the ten most successful models could be reduced – can be considered as a close approximation to the regime in the limit of zero volume fraction, *i.e.*  $\phi \rightarrow 0$ , for the case of the pick-up Reynolds number. If the same functional form is assumed to hold for the deposition velocity, which is the subject of this study, then the following expression is obtained:

$$Re_{pc} = aAr^b g(\phi, \phi_c, d, D, \rho_s, \rho_l, \nu, C_D), \quad [10]$$

where  $a$  and  $b$  are constants to be determined, as is the functional form of  $g$ .

Several putative properties of the functional form of  $g$  can be posited from the outset, based on the available data. These properties, and corresponding constraints for the form of  $g$ , are described below, and the ability of several function forms, many of which are taken from existing models described in the review of Soepyan *et al.* (2014), is discussed later and summarised in Table 4. A schematic representation of the form of  $g$ , based on the relevant literature (Davies, 1987; Gillies *et al.*, 2000; Graf *et al.*, 1970; Kökpınar and Göğüş, 2001; Parzonka *et al.*, 1981; Spells, 1955; Thomas, 1962), is shown in Figure 1.

First, the value of  $g$  in the limit of zero volume fraction,  $g_0$ , should be unity, *i.e.*

$$g_0 = 1, \quad [11]$$

so that the following expression is obtained in that limit, by analogy to Equation [7]:

$$Re_{pc0} = aAr^b. \quad [12]$$

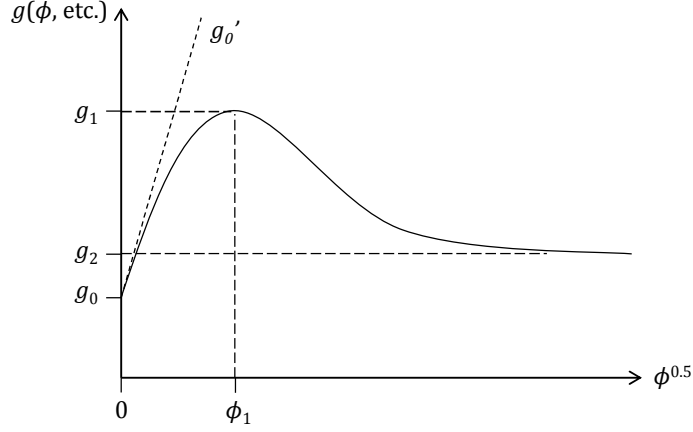


Figure 1: Schematic of functional form of  $g$  with respect to volume fraction,  $\phi$ .

Experimentally,  $Re_{pc0}$  can be estimated by extrapolation of measured data at low  $\phi$  to  $\phi = 0$ . Second, at low volume fractions (*i.e.*  $\phi \sim$  a few per cent),  $g$  varies as follows (Thomas, 1962):

$$g \approx \alpha \phi^{0.5} + \beta, \quad [13]$$

where  $\beta = 1$ , in order that the first condition (Equation [11]) be satisfied. Although the form of the dependence of  $g$  on  $\phi$  (*i.e.*  $g \propto \phi^{0.5}$ ) is tentative, it can be seen in the results section that the fit is very good (and certainly better than a  $g \propto \phi$  dependence). The value of  $\alpha$  can then be found by a simple fit of measured data, since it can be shown that:

$$\alpha = \left. \frac{Re'_{pc}}{Re_{pc}} \right|_0, \quad [14]$$

if the substitution  $p = \phi^{0.5}$  is made, such that  $Re_{pc} = Re_{pc}(p)$  in Equation [14]. The relationship expressed in Equation [14] applies equally to  $U_c$  or  $Fr_c$ , for example, as it does to  $Re_{pc}$ . Third,  $g$  reaches a maximum,  $g_1$ , at a corresponding volume fraction,  $\phi_1$ , which can “be explained on the basis of hindered settling which becomes more pronounced as concentration increases” (Turian *et al.*, 1987) or “might be related to a relative importance between long range hydrodynamic interactions associated with settling and the turbulent energy dissipation due to particles” (Poloski *et al.*, 2010) and implies that:

$$g'_1 = g'(\phi_1) = 0. \quad [15]$$

Although sometimes approximated as  $\phi_1 = 0.15$  (Poloski *et al.*, 2010),  $\phi_1$  appears to

depend on particle properties and pipe diameter quite strongly, with measured values in the range  $0.05 \lesssim \phi \lesssim 0.2$  (Parzonka *et al.*, 1981; Sinclair, 1962). Fourth,  $g$  tends to an approximately constant, positive, non-zero value at higher volume fractions (Davies, 1987; Gillies *et al.*, 2000; Kökpınar and Göğüş, 2001; Parzonka *et al.*, 1981). This is a “soft” condition, so an appropriate mathematical description would be as follows:

$$g_2'' = g''(\phi \rightarrow 1) \approx 0. \quad [16]$$

In general,  $\alpha$ ,  $\phi_1$ ,  $g_1$  and  $g_2$  should be assumed to be functions of the particle and flow properties. In fact, the value of  $g_2$  appears to depend strongly on the width of the particle size distribution (Davies, 1987; Gillies *et al.*, 2000; Parzonka *et al.*, 1981), and not only the mean particle size.

Combining Equations [10] and [13], the following for  $Re_{pc}$  at low volume fractions is obtained:

$$Re_{pc} = aAr^b(\alpha\phi^{0.5} + 1), \quad [17]$$

where  $a$ ,  $b$  and  $\alpha$  are not known. The determination of  $a$ ,  $b$  and  $\alpha$  for the critical deposition velocity in horizontal flow of solid-liquid suspensions in pipes is the main objective of the present study. This objective is separated into two parts: first, determining  $a$  and  $b$  in the limit of zero volume fraction by extrapolation of experimental data *via* Equation [12]; and second, determining  $\alpha$  by fitting of the same experimental data at low volume fractions *via* Equation [14].

### 3. Method and materials

The material properties of the four particle species used in this study are described Section 3.1; the flow loop and the ultrasonic measurement system and method are described in Section 3.2; and the method for measuring the settled bed depth and critical deposition velocity, as well as the bed geometry and other related issues, are described in Section 3.3.

#### 3.1 Materials and characterisation

Four particle species were used in this study, two glass and two plastic, the physical

properties of which are summarised in Table 2. They were chosen as they are non-hazardous and cover a range of sizes, densities, shapes and, therefore, maximum packing fractions and Archimedes numbers, where the latter is as defined in Equation [3]. The particle size was measured using *Mastersizer 2000* and *3000* laser diffraction sizers (Malvern Instruments) and the density using an *AccuPyc 1300* pycnometer (Micromeritics).

The maximum packing fraction, which must be known in order that a correction to the measured bed depth due to ambient sediment can be made, as described in detail in Section 3.3, was measured manually using standard volumetric flasks and scales: known volumes were weighed and the packing fraction calculated using the measured particle densities. To minimise wall effects – that is, the tendency of vessel walls to influence the measured packing fraction if the vessel’s size is similar to that of the particle diameter – a mean value for  $\phi_m$  was taken using at least three flasks of different volumes (50, 100, 250 and 500 ml). No trend in  $\phi_m$  with flask size was observed, confirming wall effects were not significant.

Particle type	Mean particle size, $d_{50}$ ( $\mu\text{m}$ )	Density, $\rho_s$ ( $10^3 \text{ kg m}^{-3}$ )	Max. packing fraction, $\phi_m$	Archimedes number, Ar	Shape
Small glass (Honite 22)	41.1	2.45	0.619	0.977	Spherical
Large glass (Honite 16)	77.0	2.46	0.616	6.54	Spherical
Small plastic (Guyblast 40/60)	468	1.54	0.514	539	Angular
Large plastic (Guyblast 30/40)	691	1.52	0.512	1680	Angular

It is interesting to note that the measured values of  $\phi_m$  presented in Table 2 agree well, broadly speaking, with values given by Brouwers (2006, 2014), *e.g.* the values for  $\phi_m$  of (monosized) two kinds of sand (sphericity = 0.86 and 0.81), “fairly angular” quartz and “distinctly angular” sillimanite are given as 0.624, 0.574, 0.503 and 0.469, respectively. All the values of  $\phi_m$  measured in this study (see Table 2) fall within this range, and the significance of packing is discussed further in Section 4.1.

### 3.2 Flow loop and acoustic measurement apparatus

Based on a number of criteria (cost, portability and ability to operate remotely, ease of operation and computational requirements), an ultrasonic system was chosen for the present study, consisting of a *UVP-DUO* signal processor (Met-Flow, Switzerland) and a monostatic (*i.e.* emitter-receiver) transducer (Imasonic, France) of the pencil type with a circular active face of diameter 5 mm operating at 4 MHz. The transducer was mounted, perpendicular to the mean flow direction, on a horizontal test section of a recirculating pipe flow loop (Figure 2) with an inner diameter of  $D = 42.6$  mm; the transducer was in contact with the flow *via* a hole drilled through the pipe and mounting. A variable centrifugal pump was used to control the flow rate, an impeller mixer to maintain a suspension in the mixing tank (nominal capacity 100 litres, *i.e.*  $0.1 \text{ m}^3$ ) and an electromagnetic flow meter to measure the flow rate,  $Q$ . The flow loop was filled with suspensions of each of the four particle species listed in Table 2 at several nominal (weighed) concentrations,  $\phi_w$ , and run over a range of flow rates. The fluid used in all experiments was mains water.

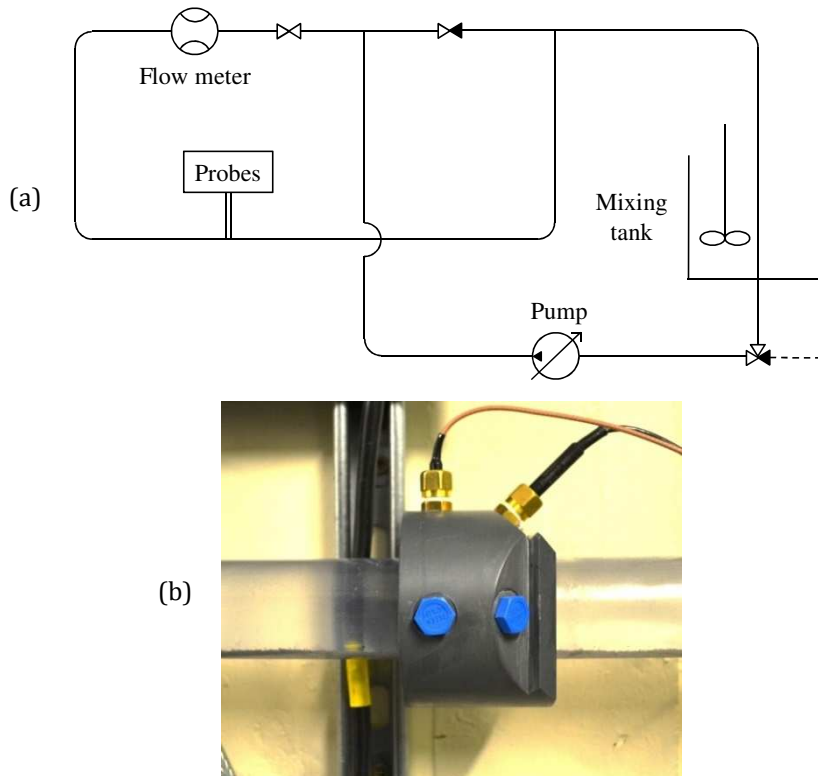


Figure 2: (a) Pipe flow loop schematic, (b) photograph of probe mounting (colour online); vertical probe only used. Inner diameter,  $D = 42.6$  mm; entry length,  $L = 3.2$  m.

The mean flow velocity,  $U_{ave}$ , was calculated from the recorded flow rate,  $Q$ , as follows:

$$U_{ave} = \frac{Q}{A} = \frac{4Q}{\pi D^2}, \quad [18]$$

where  $A$  and  $D$  are the cross-sectional area and diameter of the pipe, respectively.

For each particle species, three nominal (*i.e.* total weighed) volume fractions were used:  $\phi_w = 0.5, 1$  and  $3\%$ . For all the runs in the main pipe flow loop,  $n = 2,500$  echo data were taken for each run using the *UVP-DUO* instrument. The root-mean-square (RMS) of the instantaneous echo data at each measurement channel was taken using custom-written MATLAB scripts, and a three-sigma noise filter was applied.

A diagram of the geometry of the measurement points generated by the *UVP-DUO* system is shown in Figure 3, in which:  $r$  is the axial distance from the active face of the transducer;  $r_0$  and  $r_{max}$  are the minimum and maximum measurement distances, respectively;  $w$  is the width of each measurement channel;  $s$  is the separation between the central points of adjacent measurement channels; and  $\gamma_0$  is the beam divergence angle. The following values of these parameters were used in the present study:  $r_0 = 5$  mm;  $r_{max} = 50$  mm;  $w = s = 0.37$  mm; and  $\gamma_0 = 2.16$  degrees. Of these,  $r_0$ ,  $r_{max}$ ,  $s$  and  $w$  are adjustable to some degree, while  $\gamma_0$  is not and is dictated by the geometry of the pressure field, and therefore the size and shape of the transducer, both of which are fixed (Hay and Sheng, 1992; *Met-Flow*, 2002).

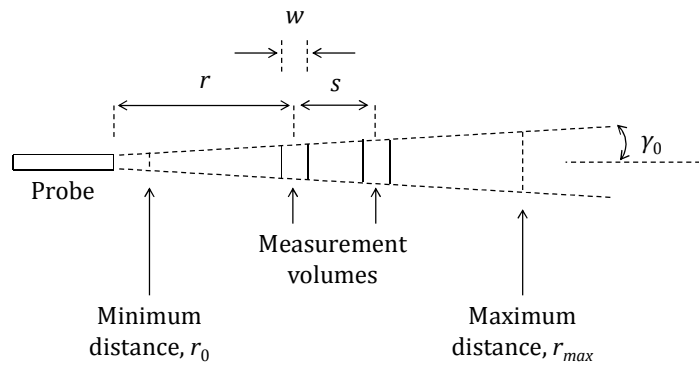


Figure 3: Schematic diagram of measurement points. Distance to centre of measurement channel, *i.e.* distance to nominal measurement point, is  $r$ ; distance between measurement points is  $s$ ; width of each measurement volume is  $w$ . Minimum and maximum distances are  $r_0$  and  $r_{max}$ , respectively. Beam divergence angle is  $\gamma_0$ .

### 3.3 Critical deposition velocity: measurement method

The method used to determine the critical deposition velocity relies on measurement of

the depth of settled beds of particles along the bottom of the pipe. This section begins, therefore, with a description of the geometry of settled beds, followed by a description of the acoustic method used to measure bed depths and a derivation of a correction to the bed depth to account for ambient suspended particles. A cross-sectional diagram of the flow and bed geometry is presented in Figure 4. The variables  $R$  and  $D$  are the radius and diameter of the pipe, respectively ( $R = 21.3$  mm,  $D = 42.6$  mm);  $h$  and  $H$  are the bed and flow depths such that:

$$D = h + H. \quad [19]$$

The variables  $A_{\text{flow}}$  and  $A_{\text{bed}}$  are the cross-sectional areas occupied by the flow and the bed, respectively, such that:

$$A = A_{\text{bed}} + A_{\text{flow}}. \quad [20]$$

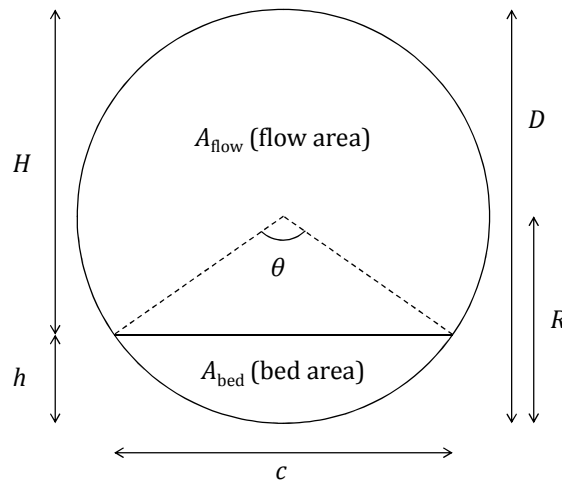


Figure 4: Diagram of flow and bed geometry.  $H$  and  $h$  are fluid and bed depths, respectively;  $R$  and  $D$  are pipe radius and diameter;  $\theta$  is angle subtended by bed at pipe centre; and  $c$  is chord length (*i.e.* bed width at top of bed).  $A_{\text{flow}}$  and  $A_{\text{bed}}$  are cross-sectional areas occupied by flow and bed, respectively.

The width of the top of the bed,  $c$ , is a chord such that:

$$c = 2\sqrt{h(2R - h)} = 2R \sin(\theta/2), \quad [21]$$

where  $\theta$ , the angle subtended by the bed at the centre of the pipe, is:

$$\theta = 2 \cos^{-1} \left( \frac{R-h}{R} \right). \quad [22]$$

The cross-sectional areas occupied by the bed,  $A_{\text{bed}}$ , and by the flow area,  $A_{\text{flow}}$ , are then:

$$A_{\text{bed}} = \frac{1}{2} R^2 (\theta - \sin \theta), \quad [23]$$

$$A_{\text{flow}} = A - A_{\text{bed}} = R^2 \left[ \pi - \frac{1}{2} (\theta - \sin \theta) \right]. \quad [24]$$

At high flow rates, the particulate phase remains fully suspended and no vertical concentration gradient exists. At intermediate flow rates, a concentration gradient develops, and a saltating or moving bed forms along the bottom of the pipe. At low flow rates, some or all of the bed is stationary and a shear layer, spanning some or all of the pipe diameter, exists above it. In the presence of a shear layer a significant proportion of the ultrasonic energy is absorbed before it reaches the stationary part of the bed (*i.e.* the lower, immobile part of the bed), whilst at very low flow rates (at which the bed is mainly or wholly settled and the shear layer is very thin or non-existent) the top part of the bed acts as a simple reflective surface. The root-mean-square of the echo profile – referred to here as the echo amplitude – was found to reach a maximum at a certain distance from the probe. This distance was assumed to correspond to the top of the stationary bed or shear layer, depending on the flow regime.

The echo amplitude,  $E$ , is recovered by the *UVP-DUO* instrument from the root-mean-square of the received voltage,  $V$ , thus:

$$E(r) = \frac{N_d V(r)}{5} = 3.28 \times 10^4 V(r), \quad [25]$$

with  $N_d = 2^{14}$ , where  $N_d$  is the digitisation constant applied by the *UVP-DUO* instrument to the voltage data (*i.e.* 14 bytes per datum), and the factor of 5 arises because the range of received voltages is set by the instrument to  $\pm 2.5$  V.

To illustrate this method, the echo amplitude profiles at three flow rates are shown in Figure 5. In run 1, the flow rate was very high ( $Q = 3.61 \text{ l s}^{-1}$ ): the particles are fully suspended and the first peak (at measurement channel 111) corresponds to the position of the lower pipe wall and run 1 could therefore be used as a reference run. In run 2, at an

intermediate flow rate ( $Q = 0.856 \text{ l s}^{-1}$ ) a shear layer is present, the top of which corresponds to the peak in echo amplitude at channel 62. Lastly, the pump was turned off in run 3 and the moving bed and suspended sediment were allowed to settle; in this case a peak in  $E$  was observed at the top of the bed, at channel 84. The distances between channels 62 and 111, and between channels 84 and 111, were then the thicknesses of the shear layer plus the stationary and moving parts of the bed (18.13 mm) and settled bed (9.99 mm), respectively.

It is clear from Figure 5 and the preceding description of the method that determination of the shear layer thickness would require a significant amount of interpretation. At very low flow rates (*i.e.* below the threshold for incipient particle motion), it would be expected to tend to zero. On the other hand, at very high flow rates, the entire cross-section will effectively be occupied by a shear layer. To preclude the possibility of encountering such ambiguities, no attempt was made to determine the shear-layer thickness in this study. Instead, only the settled-bed thickness was measured using “stop-flow” runs, in which the flow was stopped once the bed had reached an equilibrium depth, as described below, and then a correction for ambient suspended solids that would be present in corresponding “with-flow” runs was applied.

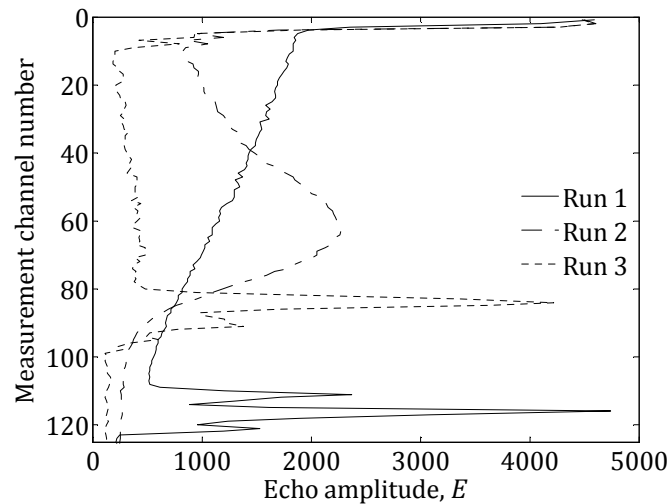


Figure 5: Echo amplitude showing peaks at three flow rates. Run 1 (solid line): high  $U_{ave}$ , fully suspended (peak at measurement channel 111); run 2 (dashed-dotted): heterogeneous flow with a shear layer (peak: 62); run 3 (dotted): stop-flow run,  $U_{ave} = 0$ , with settled bed (peak: 84).

The experimental procedure for each set of runs was as follows:

1. A mass of solids was added to the mixing tank corresponding to the nominal volume

fraction,  $\phi_w$ , and the mixer and pump turned on to generate a fully suspended flow throughout the flow loop.

2. The pump was turned to a low flow rate for several minutes, in order that a thick, stable, plane bed was generated along the horizontal test section, which was built from transparent pipe. As in all runs, the stability of the bed was determined by inspection of the echo amplitude,  $E$ , and bed depth over time.
3. The flow rate was increased incrementally ( $\Delta Q \approx 0.1 \text{ l s}^{-1}$ ), causing erosion to the top surface of the bed and a decrease in bed depth. The flow structure was allowed to reach an equilibrium state over several minutes, and then the pump was turned off and the ambient suspended sediment allowed to settle. The settled bed depth was recorded during each of these stop-flow runs.
4. The preceding step was repeated until no bed was visible along the test section.

The initial (and final) position of the particles during each measurement run is on the lower pipe wall, stationary, with the pump turned off. The critical deposition velocity corresponds to that mean flow velocity at which no bed would be present, were the pump turned on, after a bed depth correction corresponding to the ambient concentration of suspended solids has been subtracted

To summarise, the distance to the opposite pipe wall is found using a reference run, which provided a calibration distance for calculating the position of the active face of the probe relative to the inner face of the upper pipe wall. In practice, this meant the flow rate had to be high enough that the sediment was fully suspended and a settled bed (the top of which would act as a reflective surface itself) was not present. The settled bed thickness could then be calculated in a simple fashion in subsequent runs, as described above and illustrated in Figure 5.

Because the bed depths were measured during stop-flow runs, it was necessary to apply a correction,  $\delta h$ , to the bed depth to account for sediment that settles when the flow was stopped but which would remain suspended if the pump were turned on. To calculate this correction, it was assumed that the volume fraction occupied by the suspended particles,  $\phi$ , which is calculated directly from the physically sampled volume fraction,  $\phi_s$ , is equal to the area fraction occupied by the suspended particles when they settle. A further, trivial simplification – that the bed surface width,  $c$ , is constant within the depth increment  $\delta h$  – was also made such that the following expression, which also incorporates the maximum particle packing fraction,  $\phi_m$  (which was measured using the method described in Section 3.1, the results of which are presented in Table 2), can be written:

$$\phi_m c \delta h = \phi A_{\text{flow}}. \quad [26]$$

where only  $\delta h$  is unknown, and was calculated *via* Equation [26]. The uncorrected and corrected bed depths,  $h_{\text{uncorr}}$  and  $h_{\text{corr}}$ , are related as follows:

$$h_{\text{uncorr}} = h_{\text{corr}} + \delta h \quad [27]$$

The results of this technique for all four particle species over a range of flow rates and nominal volume fractions ( $\phi_w = 0.5, 1$  and  $3\%$ ) are given in the following section.

#### 4. Results and discussion

The method used to determine the critical deposition velocity is illustrated in Section 4.1 with a number of examples of the variation of bed depth versus flow velocity, one for each particle type. How these measured critical velocities were used to determine the coefficients  $a$ ,  $b$  and  $\alpha$  in Equation [17] is described in Section 4.2. An estimation of the overall experimental error associated with the method is given in Section 4.3, and some suggestions for extending the relationship between  $Re_{pc}$  and  $\phi$  to higher volume fractions are given in Section 4.4

##### 4.1 Critical flow velocity: examples

Four examples are shown below of the bed depth results, before and after the correction for ambient suspended sediment, described in Equations [26] and [27], was applied. Figure 6 shows  $U_{ave}$  versus  $h$  in the case of the small glass particles (Honite 22) at a nominal volume fraction of  $\phi_w = 0.5\%$ ; Figure 7, Figure 8 and Figure 9 show the corresponding results for the large glass particles at  $\phi_w = 3\%$ ; the small plastic particles (Guyblast 40/60) at  $\phi_w = 0.5\%$ ; and the large plastic particles (Guyblast 30/40) at  $\phi_w = 3\%$ , respectively. Using the method described in the preceding section, the critical deposition velocity was found by extrapolating the measured values of  $U_{ave}$  to zero bed depth, *i.e.*

$$U_c = U_{ave}(h = 0). \quad [28]$$

The upward “tails” observed at higher flow velocities in some of the plots arose because all data were included up to and including the flow velocity at which no bed was observed by

eye through the transparent pipework of the test section, for completeness. (The bed depth would be expected to level off at even higher flow velocities.) It is suggested that, in future, more data points could be excluded to remove these tails and thereby obtain more linear trends in the plots of bed depth,  $h$ , versus mean flow velocity,  $U_c$ . However, no general method for doing so is presented here and it is left as a subject for further study since the most appropriate exclusion of data will be specific to a particular application.

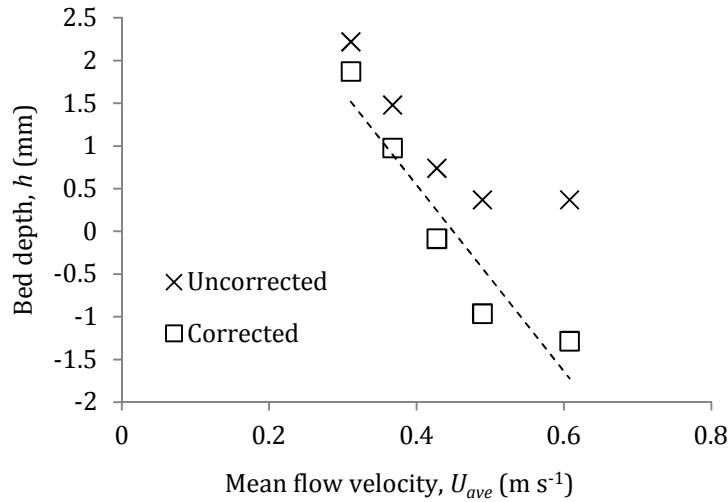


Figure 6: Bed depth,  $h$ , versus mean flow velocity,  $U_{ave}$ , with small glass particles (Honite 22) at nominal volume fraction of  $\phi_w = 0.5\%$ .

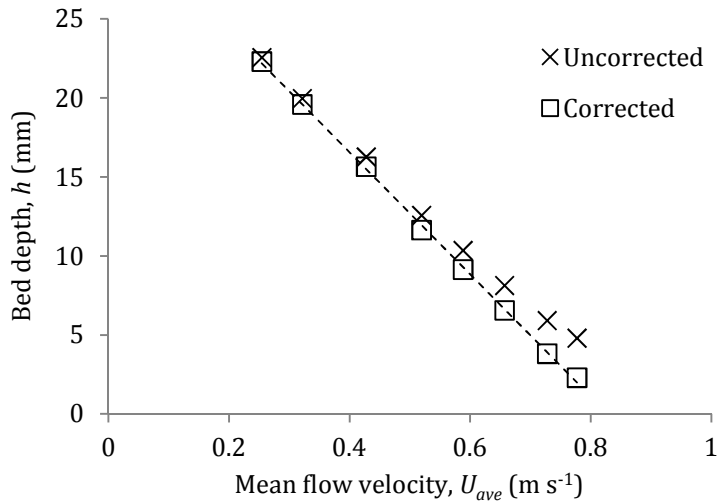


Figure 7: Bed depth,  $h$ , versus mean flow velocity,  $U_{ave}$ , with large glass particles (Honite 16) at nominal volume fraction of  $\phi_w = 3\%$ .

It is also important to explain that the correction for ambient suspended solids had a greater relative effect on the calculated bed depths at lower nominal concentrations (*e.g.* compare the large effect of the correction on a run at  $\phi_w = 0.5\%$  in Figure 6, where the

maximum bed depth is of the order of a few millimetres, to the small effect on a run at  $\phi_w = 3\%$  in Figure 7, where the maximum bed depth is of the order of tens of millimetres) simply because the bed tended to be much thinner in lower-concentration flows. The correction in absolute terms was very similar in all cases (*i.e.* up to a few millimetres).

The essence of the method is that bed depths were measured during so-called stop-flow runs – *i.e.* with the pump turned off – so that all suspended sediment settles onto the lower pipe wall. The correction accounts for the proportion of the settled bed that would not be present, were the pump turned back on. This method was devised to avoid ambiguities relating to the shear-layer thickness. The negative values arise because, above the critical flow rate, no bed is present. Therefore, applying a correction for a small bed thickness that is caused by sediment that would otherwise be suspended during a with-flow run sometimes produces a negative value. A negative value effectively means that no bed would be present, were the pump turned on.

The zero-bed-depth method is what could be called a “bottom-up” method, *i.e.* the flow rate is *increased* incrementally until the bed is eroded to nothing. A “top-down” method could be used (and, in fact, was tested), in which the flow rate is *decreased* incrementally, but the critical flow rate at which a bed begins to form would be (and was, when tested) much more difficult to determine. With the method presented here, there is an unambiguous point at which no particles remain in the bed, and that point is determined by extrapolating to zero bed depth.

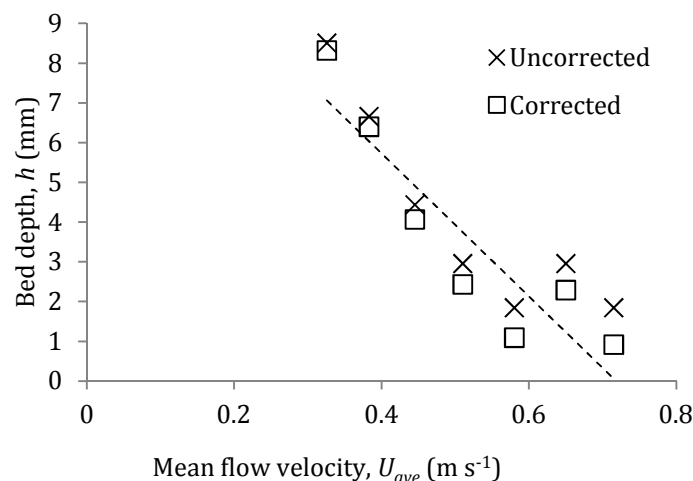


Figure 8: Bed depth,  $h$ , versus mean flow velocity,  $U_{ave}$ , with small plastic particles (Guyblast 40/60) at nominal volume fraction of  $\phi_w = 0.5\%$ .

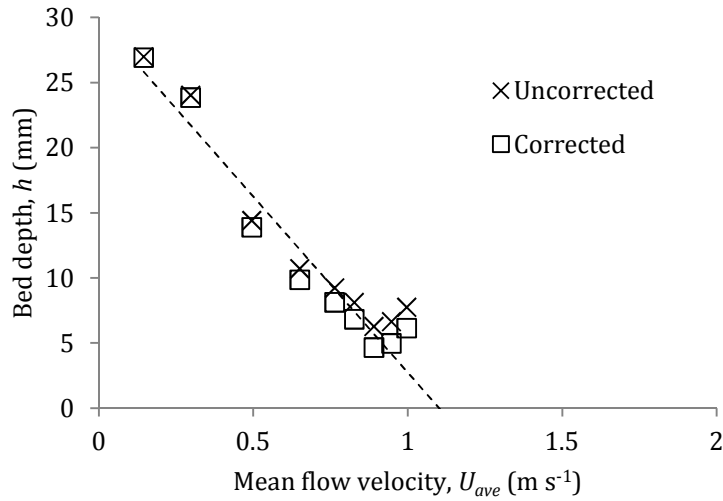


Figure 9: Bed depth,  $h$ , versus mean flow velocity,  $U_{ave}$ , with large plastic particles (Guyblast 30/40) at nominal volume fraction of  $\phi_w = 3\%$ .

A related issue is that of the maximum particle packing fractions given in Table 2. As discussed in Section 3.1, the measured values of  $\phi_m$  compared well with some values given by Brouwers (2006, 2014) for several types of mineral particles. However, because the values given in Table 2 were measured with dry particles in air, and because the effect of buoyancy in real, wetted, settled beds in the flow loop means that the packing fraction in that case may be slightly lower, it is reasonable to conclude that the dry values may not be conservative. That is, the beds in the flow loop may have been more loosely packed, and so the corrections that were made to  $h$  may have been underestimated; more conservative estimates of  $\delta h$  would lead to even greater linearity in the corrected plots of  $h$  versus  $U$  (examples of which are given in Figure 6 to Figure 9). In fact, both the measured dry values and real wetted values would be expected to fall somewhere between the random loose packing (RLP) and random close packing (RCP) limits, the former somewhat closer to the RCP and the latter somewhat closer to the RLP.

The measured values of the critical deposition velocity,  $U_c$ , are plotted versus the square root of the nominal volume fraction,  $\phi_w$ , in Figure 10 for all four particle types, according to Equation [13], using data collated at nominal volume fraction of  $\phi_w = 0.5, 1$  and  $3\%$  (including additional runs not shown in Figure 6 to Figure 9 for brevity). At such low concentrations,  $U_c$  is proportional to the square root of  $\phi_w$ . Linear fits to the data are also shown, and it is clear that the measured values of  $U_c$  followed the expected trends, increasing with both concentration and Archimedes number (see Table 2). It is also important to note that this point that the goodness of fit for the  $\phi_w^{0.5}$  dependence shown in Figure 10 was much better ( $R^2 = 0.861, 0.995, 0.993$  and  $0.999$  for small glass, large glass,

small plastic and large plastic, respectively), than for a  $\phi_w$  dependence ( $R^2 = 0.792, 0.974, 0.969$  and  $0.989$ ), which strengthens the case for the choice of functional form given tentatively in Equation [13].

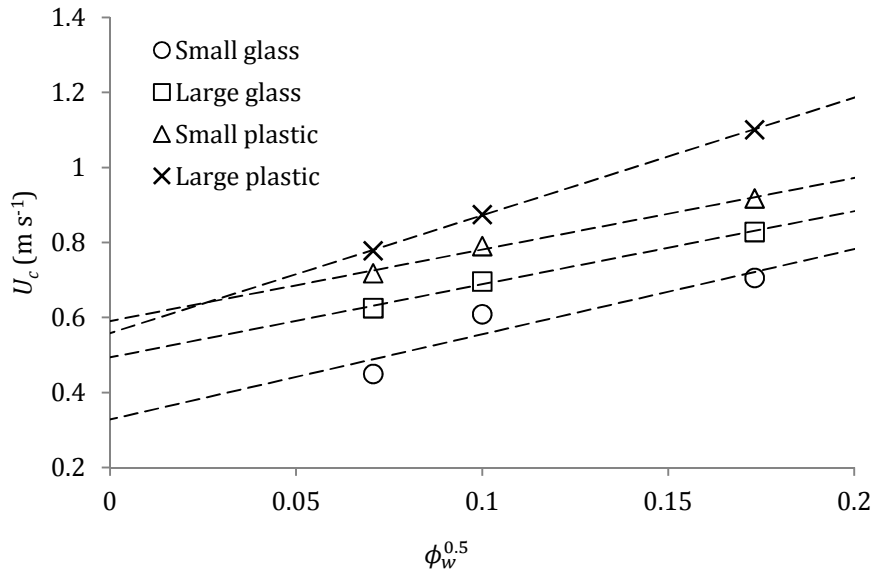


Figure 10: Limit deposition velocity,  $U_c$ , versus nominal volume fraction,  $\phi_w$ , for four particle species. Linear fits shown, for estimation of  $Re_{pc0}$  and  $\alpha$  (see text).

#### 4.2 Determination of functional coefficients

With reference to the critical deposition velocities shown in Figure 10, the critical deposition velocity in the limit  $\phi \rightarrow 0$ ,  $U_{c0}$ , was estimated by extrapolating the measured values of  $U_c$  to  $\phi = 0$ , *via* Equation [6], then converted to  $Re_{pc0}$  *via* Equation [2]. The values of  $\alpha$  for each particle species could also be computed from the intercept and gradient of the fits, *via* Equation [14]. The literature was searched for data suitable for comparison against, and compilation with, the data generated in the present study. The following selection criteria were applied, with justifications given in each case:

1. At least three data points at several volume fractions must be available, to ensure a reliable fit and accurate extrapolation to  $\phi = 0$ .
2. The data must be at low volume fractions, *i.e.* no more than a few per cent. It is not possible to be more specific, as the range over which Equation [13] is applicable is expected to depend on the particle and flow properties.
3. At least two particle size data, and preferably the full size distribution, must be available, so that the distribution is known (in the former case) or can be inferred/approximated (in the latter), *e.g.* using a normal or log-normal fit. A

consistent method for the parameterisation of the width of particle size distributions has been given by Thorne and Meral (2008).

4. The data must be specifically deposition velocity data, defined as that at which the particle phase is fully suspended, rather than for, say, the pick-up or saltation velocity.

Although the maximum packing fraction,  $\phi_m$ , is expected to be an important parameter in any universal expression for  $Re_{pc}$ , it is not included in the criteria above because it can, in general, be estimated from the available size distribution data using a suitable model (Brouwers, 2014; Hao and Riman, 2003; Ouchiya and Tanaka, 1981; Sudduth, 1993).

There is a very large amount of critical deposition velocity data available in the literature, perhaps running into thousands (Oroskar and Turian, 1980; Soepyan *et al.*, 2014; Turian *et al.*, 1997). However, very few could be found that satisfied the four criteria given above. Those that did are summarised in Table 3, along with the four data from the present study. All are plotted in Figure 11. Table 3 is intended to serve as the basis for a larger database of similar data.

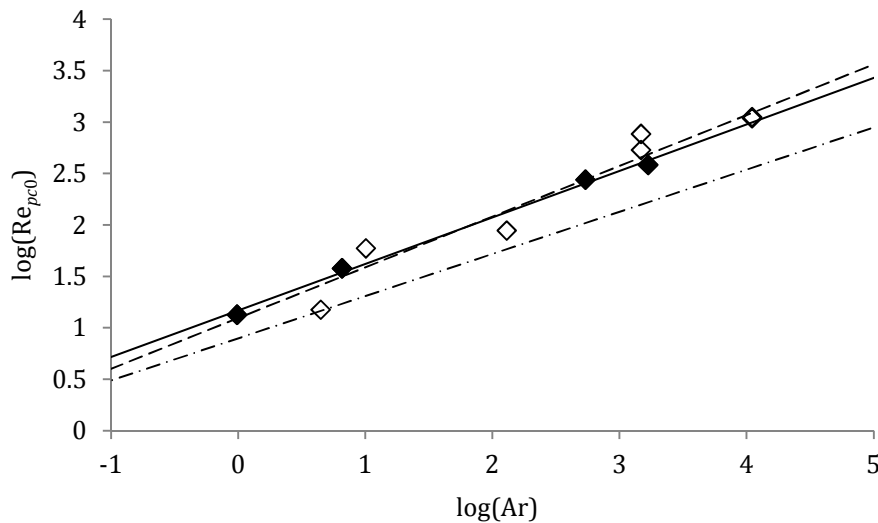


Figure 11: Variation of critical particle Reynolds number in the limit of zero concentration,  $Re_{pc0}$ , versus Archimedes number,  $Ar$ . Closed diamonds: present data; open diamonds: all data given in Table 3. Solid line: fit to present data; dashed line: fit to all data in Table 3. Dashed-dotted (lower) line: pick-up ( $Re_{pp0}$ ) correlation of Soepyan *et al.* (2014), Equation [7].

When plotted and fitted to the form of Equation [17], the resulting relationship between the particle Reynolds number corresponding to the critical deposition velocity and the Archimedes number at low concentrations (*i.e.*  $\phi$  less than a few per cent) for the four data

points obtained during the present study, all of which are given in Table 3 and are shown in Figure 11, is as follows:

$$\text{Re}_{pc} = 14.8\text{Ar}^{0.452}(1 + 4.93\phi^{0.5}). \quad [29]$$

The corresponding expression for all the data shown in Table 3 (including those obtained during this study) is:

$$\text{Re}_{pc} = 12.4\text{Ar}^{0.493}(1 + 8.91\phi^{0.5}). \quad [30]$$

By comparing Equations [29] and [30] to Equation [7], it is clear that the expressions for the deposition velocity derived in the present study yield consistently higher values than for the pick-up velocity correlation of Soepyan *et al.* (2014), as would be expected: the flow rate necessary to keep all particles suspended (*i.e.* the critical deposition velocity) exceeds that necessary to cause a particle to move from rest (*i.e.* the pick-up velocity). Mean values for  $\alpha$  over the corresponding datasets are given explicitly in Equations [29] and [30] ( $\alpha = 4.93$  and  $8.91$ , respectively). However, in general  $\alpha$  should be assumed to be a function of the material and flow properties, and it is clear from Table 3 that the values of  $\alpha$  derived in the present study and taken from the literature span an order of magnitude.

Lastly, the critical deposition Reynolds numbers and their dependence on particle volume fraction, as measured experimentally in this study, the same data as shown in Figure 10, are compared against values predicted by Equations [29] and [30] in Figure 12 and Figure 13 for the two glass and two plastic particles, respectively. In every case, it is clear that the values of  $\text{Re}_{pc}$  calculated according to Equation [29] very closely match the experimentally determined values, as would be expected: the coefficients in Equation [29] were derived from those same data. However, the match with the values calculated according to Equation [30] is not as good, which is also to be expected: as can be seen from Table 3, the values of  $\alpha$  for the datasets from the present study are all significantly lower than the average of all datasets (*i.e.*  $8.91$ ). In other words, the datasets taken from the literature exhibit a stronger dependence, on average, on particle volume fraction.

However, with so few suitable datasets available (seven from the literature, 11 in total), it is not possible to determine which variables are responsible for the observed scatter in  $\alpha$ , and by inspection of Table 3 there does not appear to be any trend in conduit diameter,

particle size or particle density. It is important to note at this point that a significant proportion of the models considered by Soepyan *et al.* (2014) include terms for particle size and density, and extensions of the procedure presented in the present study should include an analysis of these dependences, although they may be quite weak ( $O(10^{-1})$ ).

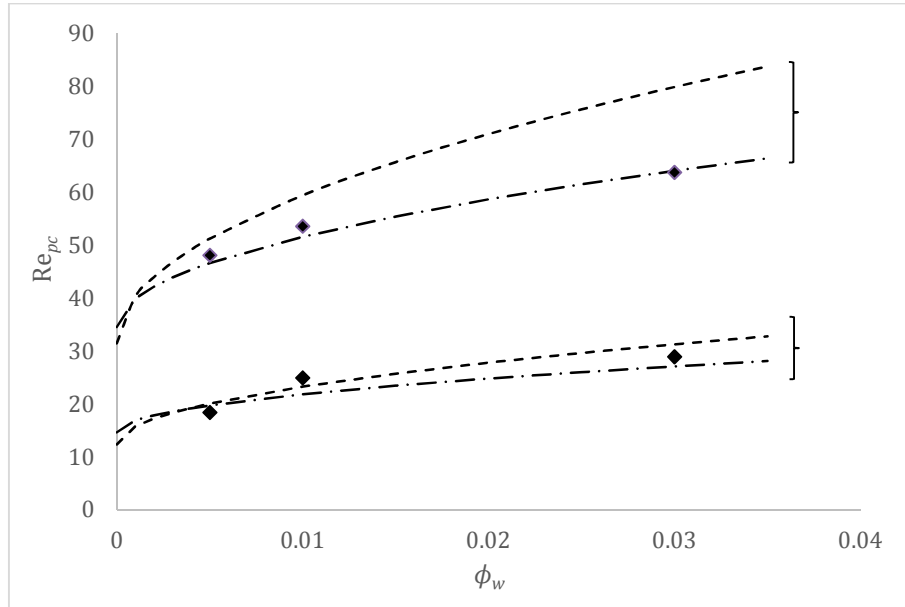


Figure 12: Comparison of experimentally determined critical deposition Reynolds number,  $Re_{pc}$ , versus nominal particle volume fraction,  $\phi_w$ , with values predicted by Equations [29] and [30] for glass particle species. Filled diamonds: this study, experimental; dashed-dotted line: Equation [29]; dashed lines: Equation [30]. Lower set (indicated by brace): small glass particles (Honite 22); upper set: large glass (Honite 16).

The data compiled in this study are insufficient for any further conclusions to be drawn on the value of the exponents of the Archimedes number in Equations [7], [29] and [30]. On one hand, the four new data from this study yielded an exponent of  $b = 0.452$ , which is close to the value of  $b = 0.41$  given by the optimisation procedure of Soepyan *et al.* (2014) for a large number (117) of pick-up velocity data, and to the value of  $b = 3/7$  (*i.e.* 0.429) found to be most appropriate for a variety of transition velocities for both pneumatic and hydraulic conveying by Rabinovich and Kalman (2011), suggesting that similar physical mechanisms are dominant. On the other hand, the value of  $b$  derived for all the data compiled here ( $b = 0.493$ ) is very close to 0.5 – *i.e.* a simple square root, suggesting that a single mechanism may be dominant – and it may be that the exponent tends to this value once more data are added to the database.

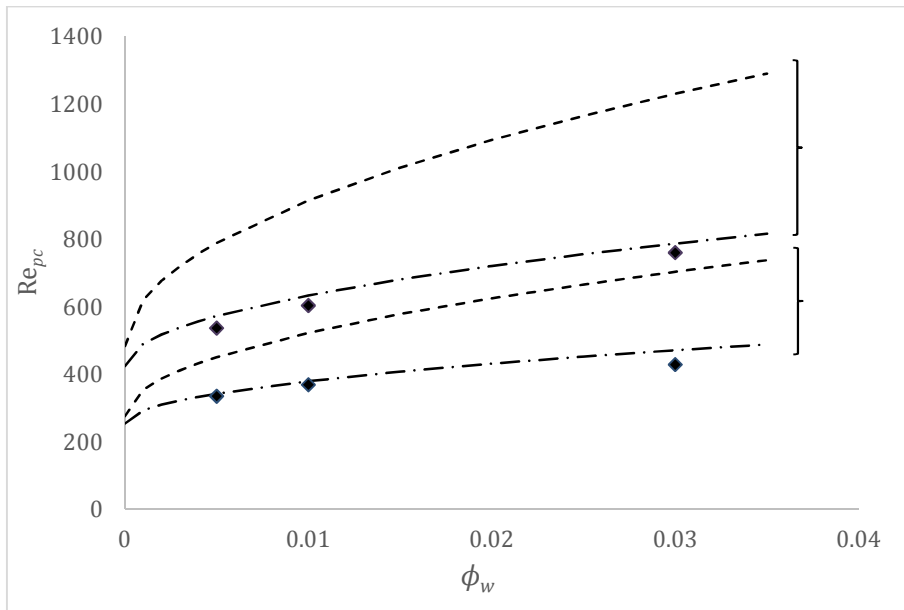


Figure 13: Comparison of experimentally determined critical deposition Reynolds number,  $Re_{pc}$ , versus nominal particle volume fraction,  $\phi_w$ , with values predicted by Equations [29] and [30] for plastic particle species. Filled diamonds: this study, experimental; dashed-dotted line: Equation [29]; dashed line: Equation [30]. Lower set (indicated by brace): small plastic particles (Guyblast 40/60); upper set: large plastic (Honite Guyblast 30/40).

Table 3: Physical properties of particle species used in correlation of $Re_{pc0}$ and Ar. Estimates of $Re_{pc0}$ and $\alpha$ , particle properties and Ar also given.									
Source	$D$ (mm)	Dataset	Particle size data ( $\mu\text{m}$ )*			$\rho$ ( $10^3 \text{ kg m}^{-3}$ )	Ar	$Re_{pc0}$	$\alpha$
Graf <i>et al.</i> (1970)	101.6	G-01	$d_{50} = 880$	$d_{90} = 1,070$	-	2.65	11,000	1,125	2.89
		G-001					11,000	1,100	3.04
	152.4	BS-01	$d_{50} = 450$	$d_{90} = 482$	-		1,470	771	1.69
		BS-001					1,470	538	5.66
Parzonka <i>et al.</i> (1981)	149	Series 6	$d_{50} = 70$	$d_{55} = 75$	-	4	10.1	59.5	6.73
		Series 8	$d_{50} = 60$	$d_{80} = 75$	-	3.1	4.45	15.0	29.6
Al-lababidi <i>et al.</i> (2012)	50	Sand	$d_{10} = 100^{**}$	$d_{50} = 200^{**}$	$d_{90} = 300^{**}$	2.65	129	88.6	28.6
Present study	42.6	Small glass	$d_{10} = 26.8$	$d_{50} = 41.1$	$d_{90} = 56.6$	2.45	0.977	13.4	6.93
		Large glass	$d_{10} = 53.5$	$d_{50} = 77.0$	$d_{90} = 104$	2.46	6.54	38.0	3.95
		Small plastic	$d_{10} = 269$	$d_{50} = 468$	$d_{90} = 712$	1.54	539	276	3.23
		Large plastic	$d_{10} = 459$	$d_{50} = 691$	$d_{90} = 966$	1.52	1680	386	5.62
* Only two data given where more were not available.									
** Estimates, bimodal particle species.									

### 4.3 Estimation of experimental errors

In order to assess the overall uncertainty associated with the zero-bed-depth method presented in this study, the relative error in  $U_{c0}$  was estimated for the four example datasets shown in Figure 6 to Figure 9. Assuming any errors in  $Re_{pc0}$  are due to errors in  $U_c$ , and neglecting all other sources of uncertainty:

$$\frac{dRe_{pc0}}{Re_{pc0}} = \frac{dU_{c0}}{U_{c0}} = \frac{dU_c}{U_c}. \quad [31]$$

To find  $dU_c$ , the data point at the highest flow rate in each dataset was excluded, and the resulting value of  $U_c$  was found in the usual way by interception with the abscissa;  $dU_c$  was then calculated to be the difference between this value and the nominal value of  $U_c$ , *i.e.* that calculated with all data included. In this way, the influence of appropriate data selection could also be assessed. From the four example datasets given in Figure 6 to Figure 9, the mean value of  $dRe_{pc0}/Re_{pc0}$  – *i.e.* the relative error in  $Re_{pc0}$  – was found to be 3.8 %.

Gillies *et al.* (2000) have noted that “deposition velocities are difficult to determine with precision”, and although the accuracy of the experimental methods used in the five studies considered by Soepyan *et al.* (2014) in order to derive Equation [7] for the pick-up velocity ranged between 0.5 and 3 %, it is thought that the method for measuring the critical deposition velocity used in the present study – namely, identification of the flow velocity corresponding to zero bed depth, by extrapolation of experimental data taken over a range of bed depths – is particularly unambiguous.

With reference to the description of the various layers of multiphase flow, and the ambiguity in measuring the shear-layer thickness, *etc.*, in the methods and materials section, it is important to repeat that this ambiguity was largely avoided by measuring the settled bed thickness instead, then applying a correction for suspended solids.

### 4.4 Dependence at higher concentrations

The remit of this study was to determine the dependence of the critical deposition velocity (and the corresponding Reynolds number) on particle concentration in the limit of zero concentration and at low concentrations up to a few per cent by volume. It is, therefore, important to note that the form of  $g$  at low volume fraction presented in Equations [29] and [30] only holds at such volume fractions. However, a discussion follows of some

possible forms of the dependence at higher concentrations: either other terms are present that become roughly unity at such low concentrations, or the bracketed terms are an approximation to a more general function that applies to all volume fractions, in which case the bracketed terms should be assumed to be the first two terms of a Maclaurin series. Identifying the full range of possible functional forms that approximate to the low- $\phi$  case presented in Equations [29] and [30] is left as a subject for future study. However, a number of standardised forms, all of which are taken from existing models and most of which are described by Soepyan *et al.* (2014) in their review, are summarised in Table 4.

It is clear from Table 4 that none of the functional forms for  $g$  satisfy all the conditions specified in the introduction. Poloski *et al.* (2010), for example, suggested a form for  $g$  of type 4 with the following coefficient values:  $k_1 = 1$ ,  $k_2 = 1$ ,  $k_3 = 2$ ,  $k_4 = 3.64$  and  $k_5 = 1$ , *i.e.*

$$g = (1 - \phi)^2(1 + 3.64\phi). \quad [32]$$

Their justification for this choice of coefficients is physically realistic and based on reliable experimental data. However, the resulting form of  $g$  satisfies some of the necessary conditions given in the introduction, but not others. Condition 1 (Equation [11]) is satisfied, as  $g$  is unity in the limit  $\phi \rightarrow 0$ , but condition 2 (Equation [13]) is not. Condition 3 is satisfied, as  $g$  does indeed reach a maximum (at  $\phi_1 = 0.15$ ), and condition 4 is not satisfied, as  $g$  is zero at  $\phi \rightarrow 1$ .

Although the form of  $g$  suggested by Poloski *et al.* (2010) cannot reproduce the behaviour of  $g$  at all volume fractions, it may represent an accurate approximate solution in specific circumstances: the scope of their study was specifically small, dense particles with narrow size distributions “which are typical of the minerals industry”. This principle – that simple expressions may be very accurate in specific circumstances – should be borne in mind when proposing any functional form for  $g$ . It can be seen from Table 4 that none of the functional forms presented are able to reproduce the observed form of  $g$  over the entire range of volume fractions.

Table 4: Possible functional forms of $g$ at higher volume fractions. All forms contrived so that coefficients $k_n$ are real and positive.						
Form no.	Form type	Are conditions 1-4 satisfied if suitable choices for $k_n$ are made?*				Example(s) of models/studies using this form**
		1	2	3	4	
1	$k_1\phi^{k_2}$	No	No	No	No	Thomas (1962); Zandi and Govatos (1967); Bain and Bonnington (1970); Gruesbeck <i>et al.</i> (1979); Kökpınar and Göğüş (2001); Almutahar (2006), “initial approach”
2	$k_1(1 - k_2\phi)^{k_3}$	Yes	No	No	No	Almutahar (2006), “new approach”
2a	$k_1(1 + k_2\phi)^{k_3}$	Yes	No	No	No	Spells (1955); Almutahar (2006), “new approach”
3	$k_1\phi^{k_2}(1 - k_3\phi)^{k_4}$	No	No	Yes	No	Oroskar and Turian (1980); Turian <i>et al.</i> (1987)
3a	$k_1\phi^{k_2}(1 + k_3\phi)^{-k_4}$	No	No	Yes	No	Rose and Duckworth (1969)
4	$k_1(1 - k_2\phi)^{k_3}(1 + k_4\phi)^{k_5}$	Yes	No	Yes	No	Davies (1987); Ponagandla (2008); Poloski <i>et al.</i> (2010)
* Conditions are described in introduction section.						
** Majority of examples taken from Soeptyan <i>et al.</i> (2014).						

## 5. Conclusions

The distinction between the critical deposition velocity (and the corresponding Reynolds number) at low solids volume fractions, and that in the limit of zero volume fractions, was explored in detail. A novel method was described for measuring the critical velocity, and expressions for the corresponding particle Reynolds number,  $Re_{pc0}$ , were derived based on experimental results and data taken from the literature, with a total of 11 points used. Significantly, these expressions suggest that some commonly used correlations for critical flow velocity (and the corresponding critical Reynolds number) are not conservative and may produce underestimates by a factor of approximately two. Based on the available data, a square-root dependence of the critical deposition velocity on the particle volume fraction at low volume fractions (*i.e.* up to a few per cent, depending on the particle species) was tentatively assumed. A number of critical deposition velocity data from the literature were selected according to a stringent set of conditions. These conditions are intended to ensure completeness of data and to allow for the effect of the particle size distribution to be included in future analyses.

The error associated with the method presented here was assessed and found to amount to a few per cent (3.8 %), based on four example datasets, which is similar to a range of values (0.5-3 %) given in a recent review by Soepyan *et al.* (2014) for several studies on the pick-up velocity. It is suggested that this error could be reduced by considering only bed depths at lower flow rates, which would minimise the uncertainty due to the shear layer and/or moving bed (if present), the thicknesses of which increase with flow rate until the solids fraction is ultimately fully suspended so that the concept of a shear layer becomes invalid, and by using more conservative values for the maximum particle packing fraction.

It is noted that neither the pipe diameter nor any of various similar length scales such as fluid depth, equivalent diameter and hydraulic diameter – which, incidentally, all become identical at zero bed depth – are represented explicitly in  $Re_p$  or  $f(Ar)$ . However, it is also noted that the pipe or conduit diameter is not present in the optimised relationships found by Soepyan *et al.* (2014) between  $Re_p$  and  $Ar$  for the pick-up and incipient motion velocities for liquid-solid and gas-solid systems. Although surprising, this suggests conduit or flow diameter is not the most important parameter at very low concentrations. On the other hand, these parameters may be more important at higher concentrations. It should be reiterated here that the purpose of this study was not to present a physical model of the critical deposition velocity as such, but rather a framework for determining the

coefficients in the relationship between  $Re_{pc}$ ,  $Ar$  and  $\phi$ , whatever the form of that relationship may be, by following the form of a number of similar relationships presented by Soepyan *et al.* (2014) and extending to higher volume fractions than considered in that study ( $0 < \phi < 10^{-4}$ ).

A number of suggestions were made for the functional dependence of the critical Reynolds number at higher particle concentrations. No satisfactory form was found and the issue is left as a subject for future study, although it is suggested that extending the dependence to concentrations above a few per cent will require significant insight into the physical processes involved, and explicit consideration of the particle shape and both the form and width of the particle size distribution. It is hoped that the database of 11 data compiled and presented in this study will form the basis of a larger database that can be used to predict the critical deposition velocity for suspensions consisting of particles with a wide range of material properties that are of general engineering interest.

## Notation

$a$	Coefficient defined in Equation [12]
$b$	Coefficient defined in Equation [12]
$A$	Cross-sectional flow area, $m^2$
$A_{bed}$	Cross-sectional area occupied by flow, $m^2$
$A_{flow}$	Cross-sectional area occupied by settled bed, $m^2$
$Ar$	Archimedes number
$Ar$	Modified form of $Ar$ taking into account solid-phase volume fraction, pipe diameter and particle sphericity and shape (after Rabinovich and Kalman, 2011)
$c$	Chord length of settled bed, $m$
$C_D$	Drag coefficient of solid particles
$d$	Particle diameter, $m$
$d_{50}$	Particle diameter, 50 <sup>th</sup> percentile, $m$
$D$	Inner pipe diameter, $m$
$E$	Echo amplitude
$f$	Function incorporating dependence of $Re_{pc}$ on $Ar$
$Fr$	Froude number
$g$	Function incorporating dependence of $Re_{pc}$ on all parameters except $Ar$
$g_n$	Acceleration due to gravity, $m\ s^{-2}$
$g_0$	Value of $g$ in limit $\phi \rightarrow 0$
$g_1$	Value of $g$ at $\phi = \phi_1$

$g_2$	Value of $g$ at $\phi = \phi_2$
$g_2''$	Second derivative of $g$ at high $\phi$
$h$	Settled bed depth, m
$h_{\text{corr}}$	Correct bed depth, m
$h_{\text{uncorr}}$	Uncorrected bed depth, m
$H$	Flow depth, m
$k_n$	$n^{\text{th}}$ coefficient in relationship between $g$ and $\phi$
$n$	Number of acoustic samples per run
$N_d$	Digitisation constant
$Q$	Volumetric flow rate, $\text{m}^3 \text{s}^{-1}$
$r$	Distance from active face of acoustic transducer along transducer axis, m
$r_0$	Minimum measurement distance from transducer, m
$r_{\text{max}}$	Maximum measurement distance from transducer, m
$R$	Inner pipe radius, m
$\text{Re}_{pc}$	Particle Reynolds number corresponding to $U_c$
$\text{Re}_{pc0}$	Value of $\text{Re}_{pc}$ in limit $\phi \rightarrow 0$
$\text{Re}_{pp}$	Reynolds number corresponding to pick-up velocity
$\text{Re}_{pp0}$	Value of $\text{Re}_{pp}$ in limit $\phi \rightarrow 0$
$\text{Re}_{pt}$	Arbitrary transitional value of $\text{Re}_p$
$\text{Re}_{pt}^*$	Modified form of $\text{Re}_{pt}$ taking into account solid-phase volume fraction, pipe diameter and particle sphericity and shape (after Rabinovich and Kalman, 2011)
$s$	Separation between central points of adjacent measurement channels, m
$S$	Specific gravity of solid particles
$U$	Axial flow velocity, $\text{m s}^{-1}$
$U_{\text{ave}}$	Mean axial flow velocity, $\text{m s}^{-1}$
$U_c$	Critical deposition velocity, $\text{m s}^{-1}$
$V$	Voltage excited in transducer, V
$w$	Width of measurement channels, m

#### *Greek letters*

$\alpha$	Coefficient defined in Equation [13]
$\beta$	Coefficient defined in Equation [13]
$\gamma_0$	Acoustic beam divergence angle, rad
$\delta h$	Bed depth correction for ambient suspended solids, m
$\Delta$	Operator indicating an increment
$\theta$	Angle subtended by settled bed at pipe centre, rad

$\nu$	Kinematic viscosity of fluid phase, $\text{m}^2 \text{s}^{-1}$
$\rho_s$	Density of solid phase, $\text{kg m}^{-3}$
$\rho_f$	Density of fluid phase, $\text{kg m}^{-3}$
$\phi$	Volume fraction of solid phase
$\phi_c$	Arbitrary critical solid-phase volume fraction
$\phi_m$	Maximum packing fraction of solid phase in settled bed
$\phi_{mb}$	Solid-phase volume fraction in moving bed
$\phi_s$	Physically sampled solid-phase volume fraction
$\phi_w$	Nominal (weighed) total delivered solid-phase volume fraction

### *Subscripts*

$c$	Critical value
$f$	Fluid-phase value
$p$	Corresponding to solid particle or value at pick-up
$s$	Solid-phase value
0	In limit $\phi \rightarrow 0$

### **Acknowledgements**

The present study is based on part of the Ph.D. thesis of H. P. Rice (“Transport and deposition behaviour of model slurries in closed pipe flow”, University of Leeds, 2013). The authors wish to thank the Engineering and Physical Sciences Research Council for their financial support of the work reported in this paper under EPSRC Grant EP/F055412/1, “DIAMOND: Decommissioning, Immobilisation and Management of Nuclear Wastes for Disposal”. The authors also thank Peter Dawson, Gareth Keevil and Russell Dixon for their technical assistance, and Olivier Mariette at *Met-Flow*, Switzerland, for his support and advice.

### **References**

- AL-LABABIDI, S., YAN, W. AND YEUNG, H. 2012, Sand transportations and deposition characteristics in multiphase flows in pipelines, *J. Energ. Resour. Technol.-ASME*, 134, 034501 (13 pages).
- ALMUTAHAR, F. M. 2006, *Modeling of critical deposition velocities of sand in horizontal and inclined pipes*, M.S., University of Tulsa.
- BAIN, A. G. AND BONNINGTON, S. T. 1970, *The hydraulic transport of solids by pipeline*, Pergamon Press.

- BROUWERS, H. J. H. 2006, Particle-size distribution and packing fraction of geometric random packings, *Phys. Rev. E*, 74, 031309.
- BROUWERS, H. J. H. 2014, Packing fraction of particles with lognormal size distribution, *Phys. Rev. E*, 89, 052211.
- CROWE, C. T. 2006, *Multiphase Flow Handbook*, Boca Raton, CRC Press, Taylor & Francis.
- DAVIES, J. T. 1987, Calculation of critical velocities to maintain solids in suspension in horizontal pipes, *Chem. Eng. Sci.*, 42, 1667-1670.
- DEY, S. 1999, Sediment threshold, *Appl. Math. Model.*, 23, 399-417.
- DORON, P. AND BARNEA, D. 1995, Pressure drop and limit deposit velocity for solid-liquid flow in pipes, *Chem. Eng. Sci.*, 50, 1595-1604.
- DORON, P. AND BARNEA, D. 1996, Flow pattern maps for solid-liquid flow in pipes, *Int. J. Multiphas. Flow*, 22, 273-283.
- GILLIES, R. G., SCHAAN, J., SUMNER, R. J., MCKIBBEN, M. J. AND SHOOK, C. A. 2000, Deposition velocities for Newtonian slurries in turbulent flow, *Can. J. Chem. Eng.*, 78, 704-708.
- GILLIES, R. G. AND SHOOK, C. A. 1991, A deposition velocity correlation for water slurries, *Can. J. Chem. Eng.*, 69, 1225-1228.
- GRAF, W. H., ROBINSON, M. P. AND YUCEL, O. 1970. Critical velocity for solid-liquid mixtures, Fritz Laboratory Reports, Paper 386. Bethlehem, PA: Lehigh University.
- GRUESBECK, C., SALATHIEL, W. M. AND ECHOLS, E. E. 1979, Design of gravel packs in deviated wellbores, *J. Petrol. Technol.*, 31, 109-115.
- HAO, T. AND RIMAN, R. E. 2003, Methodology for determination of the maximum packing fraction for particle-filled polymer suspensions, *Particul. Sci. Technol.*, 21, 317-325.
- HARBOTTLE, D., FAIRWEATHER, M. AND BIGGS, S. 2011, The minimum transport velocity of colloidal silica suspensions, *Chem. Eng. Sci.*, 66, 2309-2316.
- HAY, A. E. AND SHENG, J. Y. 1992, Vertical profiles of suspended sand concentration and size from multifrequency acoustic backscatter, *J. Geophys. Res.-Oceans*, 97, 15661-15677.
- HAYDEN, K. S., PARK, K. AND CURTIS, J. S. 2003, Effect of particle characteristics on particle pickup velocity, *Powder Technol.*, 131, 7-14.
- KÖKPINAR, M. A. AND GÖĞÜŞ, M. 2001, Critical flow velocity in slurry transporting horizontal pipelines, *J. Hydraul. Eng.-ASCE*, 127, 763-771.
- MANTZ, P. A. 1977, Incipient transport of fine grains and flakes by fluids - extended Shields diagram, *J. Hydr. Div.-ASCE*, 103, 601-615.
- MET-FLOW 2002. UVP monitor model UVP-Duo with software version 3. Revision 5 ed. Lausanne, Switzerland: Met-Flow SA.
- OROSKAR, A. R. AND TURIAN, R. M. 1980, The critical velocity in pipeline flows of slurries, *AIChE J.*, 26, 550-558.
- OUCHIYAMA, N. AND TANAKA, T. 1981, Porosity of a mass of solid particles having a range of sizes, *Ind. Eng. Chem. Fundam.*, 20, 66-71.
- PARZONKA, W., KENCHINGTON, J. M. AND CHARLES, M. E. 1981, Hydrotransport of solids in horizontal pipes: effects of solid concentration and particle size on the deposit velocity, *Can. J. Chem. Eng.*, 59, 291-296.
- PEKER, S. M. AND HELVACI, S. S. 2007, *Solid-Liquid Two Phase Flow*, Elsevier.
- POLOSKI, A. P., ETCHELLS, A. W., CHUN, J., ADKINS, H. E., CASELLA, A. M., MINETTE, M. J. AND YOKUDA, S. T. 2010, A pipeline transport correlation for slurries with small but dense particles, *Can. J. Chem. Eng.*, 88, 182-189.

- PONAGANDLA, V. 2008, *Critical deposition velocity method for dispersed sand transport in horizontal flow*, M.S., University of Tulsa.
- RABINOVICH, E. AND KALMAN, H. 2007, Pickup, critical and wind threshold velocities of particles, *Powder Technol.*, 176, 9-17.
- RABINOVICH, E. AND KALMAN, H. 2009, Incipient motion of individual particles in horizontal particle-fluid systems: A. Experimental analysis, *Powder Technol.*, 192, 318-325.
- RABINOVICH, E. AND KALMAN, H. 2011, Threshold velocities of particle-fluid flows in horizontal pipes and ducts: literature review, *Rev. Chem. Eng.*, 27, 215-239.
- ROSE, H. E. AND DUCKWORTH, R. A. 1969, Transport of solid particles in liquid and gases, *The Engineer*, 227, 478-483.
- SINCLAIR, C. G. 1962. The limit deposit-velocity of heterogeneous suspensions. *Symposium on the Interaction between Fluids and Particles: Third Congress of the European Federation of Chemical Engineers*. London.
- SOEPPAN, F. B., CREMASCHI, S., SARICA, C., SUBRAMANI, H. J. AND KOUBA, G. E. 2014, Solids transport models comparison and fine-tuning for horizontal, low concentration flow in single-phase carrier fluid, *AIChE J.*, 60, 76-112.
- SPELLS, K. E. 1955, Correlations for use in transport of aqueous suspension of fine solids through pipes, *Trans. Inst. Chem. Eng.*, 79-84.
- SUDDUTH, R. D. 1993, A new method to predict the maximum packing fraction and the viscosity of solutions with a size distribution of suspended particles. II, *J. Appl. Polym. Sci.*, 48, 37-55.
- THOMAS, D. G. 1962, Transport characteristics of suspensions: Part VI. Minimum transport velocity for large particle size suspensions in round horizontal pipes, *AIChE J.*, 8, 373-378.
- THORNE, P. D. AND MERAL, R. 2008, Formulations for the scattering properties of suspended sandy sediments for use in the application of acoustics to sediment transport processes, *Cont. Shelf Res.*, 28, 309-317.
- TURIAN, R. M., HSU, F. L. AND MA, T. W. 1987, Estimation of the critical velocity in pipeline flow in slurries, *Powder Technol.*, 51, 35-47.
- TURIAN, R. M., MA, T. W., HSU, F. L. G. AND SUNG, D. J. 1997, Characterization, settling, and rheology of concentrated fine particulate mineral slurries, *Powder Technol.*, 93, 219-233.
- WASP, E. J., KENNY, J. P. AND GANDHI, R. L. 1977, *Solid-Liquid Flow Slurry Pipeline Transportation*, Clausthal, Trans-Tech Publications.
- ZANDI, I. AND GOVATOS, G. 1967, Heterogeneous flow of solids in pipelines, *J. Hydr. Div.-ASCE*, 93 (HY3), 145-159.
- ZENZ, F. A. 1964, Conveyability of materials of mixed particle size, *Ind. Eng. Chem. Fundam.*, 3, 65-75.